Environ. Eng. Res. 2019; 24(3): 463-473
https://doi.org/10.4491/eer.2018.320

pISSN 1226-1025
eISSN 2005-968X

A cost-effective method to prepare size-controlled nanoscale zero-valent iron for nitrate reduction

Claudio Adrian Ruiz-Torres[1,2], René Fernando Araujo-Martínez[1], Gabriel Alejandro Martínez-Castañón[1], J. Elpidio Morales-Sánchez[1], Tae-Jin Lee[2], Hyun-Sang Shin[2], Yuhoon Hwang[2†], Abel Hurtado-Macías[3], Facundo Ruiz[1†]

[1]*Faculty of Sciences, The Autonomous University of San Luis Potosí (UASLP), Avenida Manuel Nava 6, Zona Universitaria, CP. 78290 San Luis Potosí, SLP., Mexico*
[2]*Department of Environmental Engineering, Seoul National University of Science and Technology, Seoul 01811, Republic of Korea*
[3]*Research Center for Advanced Materials (CIMAV), Ave. Miguel de Cervantes 120, Complejo Industrial Chihuahua, 31109 Chihuahua, Chihuahua, Mexico*

ABSTRACT

Nanoscale zero-valent iron (nZVI) has proved to be an effective tool in applied environmental nanotechnology, where the decreased particle diameter provides a drastic change in the properties and efficiency of nanomaterials used in water purification. However, the agglomeration and colloidal instability represent a problematic and a remarkable reduction in nZVI reactivity. In view of that, this study reports a simple and cost-effective new strategy for ultra-small (< 7.5%) distributed functionalized nZVI-EG (1-9 nm), with high colloidal stability and reduction capacity. These were obtained without inert conditions, using a simple, economical synthesis methodology employing two stabilization mechanisms based on the use of non-aqueous solvent (methanol) and ethylene glycol (EG) as a stabilizer. The information from UV-Vis absorption spectroscopy and Fourier transform infrared spectroscopy suggests iron ion coordination by interaction with methanol molecules. Subsequently, after nZVI formation, particle-surface modification occurs by the addition of the EG. Size distribution analysis shows an average diameter of 4.23 nm and the predominance (> 90%) of particles with sizes < 6.10 nm. Evaluation of the stability of functionalized nZVI by sedimentation test and a dynamic light-scattering technique, demonstrated very high colloidal stability. The ultra-small particles displayed a rapid and high nitrate removal capacity from water.

Keywords: Ethylene glycol, High colloidal stability, Nanoscale zero-valent iron (nZVI), Non-aqueous solvent, Stabilization mechanism, Ultra-small

1. Introduction

Alarming population growth and growing industrial activities, have led to elevated concentrations of a wide range of contaminants in wastewater and groundwater [1]. Nanoscale zero-valent iron (nZVI) has proved an effective tool for the treatment of wastewater because of their large surface area and specific affinity for toxic contaminants in aqueous systems [2]. However, the need to find materials with greater efficiency for this application persists. This improvement in efficiency is related to the dimensions and the uniformity of the diameters, and to the anti-aggregation capacity and colloidal stability, of the nanoparticles. In addition, they need to be obtained using simple and economical synthesis methodologies to become a cost-effective solution in environmental remediation.

There are several reports of nanomaterials of zero-valent iron with ultra-small size and narrow size distribution (< 3-8 nm). These were made using synthetic techniques based on sonochemical decomposition of iron carbonyl, thermal decomposition of iron pentacarbonyl, and sonolysis of iron pentacarbonyl. The methodologies made use of a stabilizing agent of variable composition (polyvinylpyrrolidone (PVP), oleic acid (OA) oleylamine (OY), poly(ethyleneglycol) (PEG)), that intensified the reduction and control of particle size [3-6]. However, the synthesis techniques mentioned above are all extremely complex and expensive meth-

Received September 6, 2018 **Accepted** November 2, 2018

† Corresponding author
Email: yhhwang@seoultech.ac.kr, facundo@fciencias.uaslp.mx
Tel: +82-2-970-6626, +52-444-826-2468 Fax: +82-2-971-5776, +52-444-826-2321
ORCID: 0000-0002-4013-3989 (Y. Hwang)

odologies that require tightly controlled conditions. This makes it hard to use nZVI as a decontamination agent for environmental purification in real applications.

In light of this, in this work, emphasis was placed on the chemical reduction of a ferric salt ($FeCl_3$) in aqueous phase, using sodium borohydride ($NaBH_4$) as reducing agent [7]. This results in a remarkable reduction in costs and complexity. However, corrosion during synthesis should be carefully controlled, which implies the need for inert conditions (Nitrogen or Argon atmosphere), complicating the methodology. Moreover, several reports have stated that this methodology results in a broad particle-size distribution, producing nanoparticles with diameters in the range 10-100 nm, with average sizes of 50-70 nm. Such results proved to be characteristic of this synthesis methodology [7-11].

In order to overcome the issues mentioned above, the use of organic stabilizing agents for surface modification of the nanomaterials of this type has been studied extensively in recent years. The aim has been to modify the interactions of the particles with the surrounding environment, altering with this the dispersibility of the material in the solvent, the aggregation rate of the magnetic particles, and thus, the particles surface area available to react with the target contaminant [9, 12]. In the same way, through the use of organic substances during synthesis of the nanomaterial, it is possible to generate conditions of steric repulsion between the particles to control their size. This occurs during the formation of the primary particles in the nucleation process, and is due to the interaction between these and the chains of the polymer used. The latter are grafted onto the surface of the nanoparticles to stabilize them, thereby avoiding their agglomeration and growth, and achieving smaller particle diameters of nZVI (< 40 nm). Nevertheless, even when size reduction occurs by the use of a coated agent, on average, the particles obtained show a broad size distribution (± 2-60 nm) [13, 14]. For this reason, it is deduced that the current control is poor in this respect. In addition, in our previous study, we presented the effectiveness of ethylene glycol (EG) as functionalized agent for obtaining air-stable nZVI and achieving size-distribution control [15]. However, even with the presence of EG, particles of large diameter still occurred, which means that using this methodology is not enough to control the size of the nanoparticles. Therefore, there is still need to obtain ultra-small nanoparticles with narrow size distribution using a cost-effective, simple methodology.

In response, modification of the synthesis methodology in question regarding the type of solvent used has been studied recently. In this work, non-aqueous solvents, more specifically alcohols, were used as a substitute, providing various benefits during the synthesis of nanomaterials. There are several reports of non-aqueous solvents used for the synthesis of nanoparticles, which have demonstrated that the physical properties of the solvent are directly related to particle stabilization [16-19]. In fact, it is known that viscosity is linearly associated with molecular diffusion [20]; so the low viscosity index of alcohols, specifically that of methanol (MeOH), favors the propagation of the reducing agent and the precursor within the solvent, increasing uniformity in the reduction and nucleation process. In addition, the nanomaterials obtained by means of chemical reduction in weakly polar solvents promotes increase in the concentrations of nuclei and promotes small particle sizes [19]. One of the main benefits in the use of non-aqueous solvents for the synthesis of zero-valent iron nanomaterials is prevention of excessive oxidation of the material. This preserves the metallic core of reactive iron and avoids the use of inert atmosphere, reducing the cost of the methodology remarkably. However, even with the use of only non-aqueous solvent, which generates smaller particle sizes as compared to aqueous synthesis, a broad distribution of sizes was reported [18]. Moreover, there are counterproductive effects from the use of alcohols as solvents, including inhibition of H-bonding that results in lower electrostatic stabilization of the nanomaterial in the solvent, which induces interaction between the particles and generation of agglomeration and growth [18]. For these reasons, the non-aqueous solvent methodologies were reported to be good methods to reduce the size of the nanoparticles, but not enough to obtain ultra-small, size controlled nZVI. Therefore, in this work, the addition of a polymeric functionalizing agent to stabilize the nanoparticles and control the agglomeration and size, was implemented by grafting EG brushes onto the surfaces of the particles. Accordingly, an implementation was proposed that involves two stabilization mechanisms associated with use of a non-aqueous solvent and a functionalizing agent. It is expected that two organic molecules, MeOH and EG, will interact in nZVI synthesis to help it grow in a controlled manner. On the other hand, owing to the magnetic attraction dominates the interaction energy in magnetic nanoparticles such as nZVI [21], the nanoparticles tend to rapidly agglomerate, limiting their mobility and stability in water, reducing their efficiency and application, mainly in the treatment of groundwater [9]. Hence the increase in the dispersibility by materials functionalization and the size reduction will produce materials with a high nanosuspension.

This work presents a method for cost-effective synthesis with size distribution < 7.5% nZVI (1-9 nm) generated using a non-aqueous chemical reduction method at room temperature without inert conditions. In addition, the synthesis of zero-valent iron nanoparticles without a coating agent (S-nZVI) was realized to compare the effects on the different materials associated with the absence and presence of the functionalization by EG. These effects included such as the decrement in the particle diameter, control of the size distribution, and the benefits of increased colloidal stability and reactivity of the nanomaterials due to the grafted polymers.

The different stabilization mechanisms involved were analyzed using ultraviolet-visible (UV-Vis) absorption spectroscopy and Fourier transform infrared spectroscopy (FTIR). The structural characterization of the materials included crystallinity, morphology, size distribution analysis, and colloidal stability. In addition, size distribution analysis was used to compare the materials obtained in this work using non-aqueous methodology ($nZVI\text{-}EG_{non\text{-}aq}$ and $S\text{-}nZVI_{non\text{-}aq}$), and those obtained via surface modified nZVI generated using aqueous methodology ($nZVI\text{-}EG_{aq}$), as presented in our previous study [15]. The advantages of using methanol as solvent were also demonstrated. The reactivity of the materials was evaluated using the quantification of reactive iron content and the nitrate reduction capacity. Similarly, in the reaction tests, different materials ($nZVI\text{-}EG_{non\text{-}aq}$, $S\text{-}nZVI_{non\text{-}aq}$, and $nZVI\text{-}EG_{aq}$) were evaluated to compare the different nitrate reduction capabilities associated with particle size and functionalization.

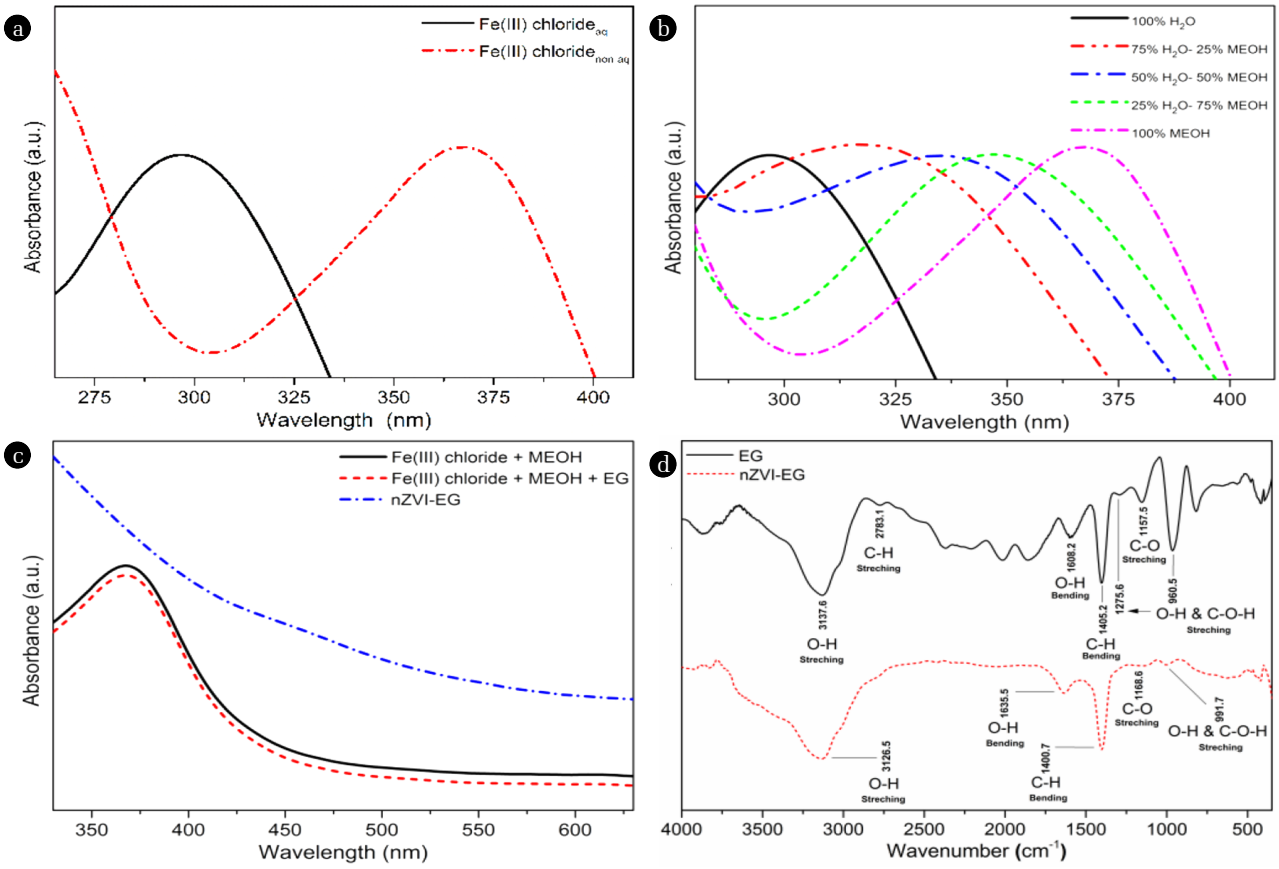

Fig. 1. a) $FeCl_3$ aqueous and non-aqueous spectrum, b) UV-Vis absorption spectra of H_2O to MEOH ratios: 100/0, 75/25, 50/50, 25/75 and 0/100%, c) $[Fe(CH_3OH)_4Cl_2]^+$ in the presence of EG and nZVI functionalized with EG spectra, d) FTIR spectrum of EG and nZVI-$EG_{non\text{-}aq}$.

2. Materials and Methods

2.1. Reagents

Ferric chloride hexahydrate ($FeCl_3 \cdot 6H_2O$) was purchased from Fermont. Sodium borohydride ($NaBH_4$), potassium nitrate (KNO_3), hydrochloric acid (HCl), and methanol (CH_3OH) were obtained from Sigma-Aldrich. Ethylene glycol (EG) was purchased from Fluka. All the chemicals used in this study were of analytical grade and were used without further purification.

2.2. nZVI Synthesis

Nanoscale zero valent iron synthesis was performed by modifying a previously proposed method [13] to provide chemical reduction of a ferric salt ($FeCl_3$) in methanol (solvent) using $NaBH_4$ as reducing agent. Initially, a Fe^{3+} solution was prepared and 0.4 mL of EG was added and mixed for 5 min at 800 r/min without inert atmosphere at room temperature. Finally, 0.05 M of the reducing agent was added to the vessel and nucleation of the EG functionalized particles was initiated. S-nZVI was prepared under similar conditions, but without EG addition during synthesis.

2.3. Physical Characterization Methods

To identify the mechanisms involved in stabilization and functionalization, coated samples were characterized by UV-Vis absorption spectroscopy using a S2000-UV-Vis spectrometer (OceanOptics, Inc.) and Fourier transform infrared spectroscopy (FTIR; Shimadzu IRAffinity-1). X-ray diffraction (XRD) data was obtained with a GBC-Difftech MMA diffractometer with filtered CuKα (λ = 1.54 A) radiation. X-ray diffraction data analysis was obtained by subjecting the XRD data to Rietveld refinement using the software MAUD. This was done to corroborate the presence of iron zero-valent (α-Fe) and iron oxide (Fe_xO_y); and to do phase quantification. The morphology was observed using transmission electron microscopy (TEM), carried out at 100 kV using a JEOL-1230. The average hydrodynamic size and Z-potential were measured with Nanosizer DLS. The sedimentation rate and colloidal stability of the produced nanoparticles, with and without functionalization, were tested by measuring optical density at 508 nm using a UV-Vis spectrophotometer (Cary 50, Agilent Technologies Inc., USA) based on the methodology reported by our previous study [9].

2.4. Reactivity Analysis

Reactivity analysis of the different materials types was determined by quantification of reactive iron contents by measuring the hydrogen (H_2) gas produced by acid digestion and nitrate reduction

[9, 22]. Evaluation of the nitrate reducing capacity of the materials was carried out using the experimental methodology reported by our previous study [23].

3. Results and Discussion

3.1. Functionalized nZVI Prepared by Non-aqueous Reduction

3.1.1. Ultraviolet-visible (UV-Vis) absorption spectroscopy

The UV-Vis absorption spectrums were analyzed in order to identify the interaction of CH_3OH molecules with Fe^{3+} during synthesis. This was compared with the characteristic cation spectra in aqueous and non-aqueous solvents under the same conditions. Fig. 2(a) displays the absorption spectrum of $FeCl_3$ in aqueous solution. A band showed at 300 nm, which corresponds to the presence of Fe^{3+} ions. In contrast, the $FeCl_3$ non-aqueous solution presented the same band at 364 nm, indicating a red-shifted band position. This was attributed to the Fe^{3+} coordination performed during interaction between iron ions and CH_3OH molecules to form a relatively stable coordination compound $[Fe(CH_3OH)_4Cl_2]^+$. In fact, there is a report of the electronic absorption spectra for iron(III) chloride in non-aqueous solvents [24]. This explains that the shift in band position (compared to that in an aqueous medium) is caused by the solvation of the salt in methanol, which generates the chemical species Cl^- and dichloro-iron(III) cation. The latter has an absorption peak at 366 nm.

In addition, absorption spectra for different concentrations of water (0, 25, 50, 75, and 100%) were analyzed with the purpose of discovering the role of methanol in Fe^{3+} coordination in relation to the red-shifted band. In Fig. 2(b) it is possible to observe that, as the methanol content increases, the band located at 300 nm shifts to 364 nm. This demonstrates that the red shift and the generation of $[Fe(CH_3OH)_4Cl_2]^+$ is directly proportional to the concentration of methanol available to react with Fe^{3+}. After the addition of the stabilizing agent EG to a non-aqueous solution, no change can be observed in the absorption spectrum. From this, it is concluded that the first mechanism of stabilization is attributable solely to the interaction between CH_3OH and Fe^{3+}. Subsequently, the addition of $NaBH_4$ caused the reduction of the complex formed and the nucleation of nZVI. In the absorption spectrum belonging to stabilized Fe-Nps (nZVI-EG), there is a modification in the absorption band that is completely different from that of the initial solution (Fig. 2(c)).

3.1.2. Fourier-transform infrared spectroscopy (FTIR)

In order to corroborate the functionalization of nZVI and to identify the mechanism involved in the second step in the stabilization of the particles, EG molecules and EG stabilized nZVI were analyzed using FTIR. These data were used to compare the vibrational frequencies associated with the functional groups present in the samples and to examine changes that occurred in the chemical bonds. Fig. 2(d) and Table S1 show the FTIR analysis and band positions (cm^{-1}) corresponding to the asymmetric vibrational modes for EG and nZVI-EG. The infrared spectra of EG display an O-H stretching vibrational mode at 3,137.6 cm^{-1}, and also at 2,783.1 cm^{-1}, where there is a sharp peak associated with C-H group asymmetric stretch-deformation. Moreover, the peak at 1,405.2 cm^{-1} is associated with the bending strain of the groups C-H contained in EG molecules. The wavenumber at 1,275.6 and 960.5 cm^{-1} is assignable to the stretching of O-H and C-O-H molecules. Finally, the band position at 1,157.5 cm^{-1} is related to the stretching of C-O groups.

In the case of nZVI-$EG_{non\text{-}aq}$, it is possible to see four principal bands (at 3,126.5, 1,400.7, 1,168.6 and 991.7 cm^{-1}) assignable to the O-H, C-H, O-H, and C-O-H stretching and flexural vibrational modes, which correspond to the characteristic vibrational frequencies of EG. In addition the wave number 991.7 cm^{-1}, which is associated with the stretching deformation of the groups O-H and C-O-H in nZVI- $EG_{non\text{-}aq}$, present a noticeable decrease in the intensity of the band in contrast with that of EG (Fig. 2(d)). This decrease in intensity is directly attributed to the metal-ligand binding, by the interaction between the O-atoms contained in the ligand molecule -OH of coated agent and Fe-atoms, by coordinated covalent bonds, thereby, decreasing the intensity of deformation by stretching of the O-H bond because of its attenuation. Indicating with this the material functionalization by EG [15, 25]. Through this effect, the polymer grafted onto particle surfaces prevents their agglomeration and growth by effects of excluded volume. The EG chains in functionalized nanoparticles are located a spatially short distance from another nZVI-EG with which repulsive interaction occurs between EG brushes. Because polymer chains cannot occupy the same space, the number of conformations that the chain can assume is reduced, in contrast to when they are at longer distances due to the superposition of the electron clouds of the molecules [26]. In a similar way, it has been widely documented that steric repulsion occurs between the nanoparticles in response to increase of the local osmotic pressure where it is established that overlap of the polymer chains occurs. This causes an increase in the concentration of the polymer in this region; compared with the solvent generating this local pressure increment. This in turn, adds to the excluded volume effect and decreases the freedom degrees of the system. This is thermodynamically infeasible, which promotes particle separation and restoration of the energy balance in the system.

3.1.3. Stabilization mechanisms

It was previously reported that the functionalization of nanoparticles using molecules with a -OH ligand group was carried out through the interaction of several stabilization mechanisms. Because methanol is an alcohol, it has an -OH ligand molecule with lone electrons pairs available; therefore, it acts as a Lewis base able to react with a Lewis acid (Fe^{3+}) by coordination. Wertz and Kruh [27] reported structures of the solute species of Fe(III) chloride with methanol in concentrated $FeCl_3$-MeOH solutions, by analyzing the dissociation of $FeCl_3{\cdot}6H_2O$ salt in non-aqueous solvent. They established a solute model to explain the solvation of iron ions in methanol, which is carried out by octahedral coordination of Fe^{3+} with four iron-oxygen bonds and two chlorine-iron bonds $[Fe(CH_3OH)_4Cl_2]^+$.

The functionalization mechanism in which EG is a stabilizing agent was previously reported [15]. Stabilization is performed by the interaction of the ligand molecule -OH contained in the EG chain with the Fe-atoms contained on the surface of the particle,

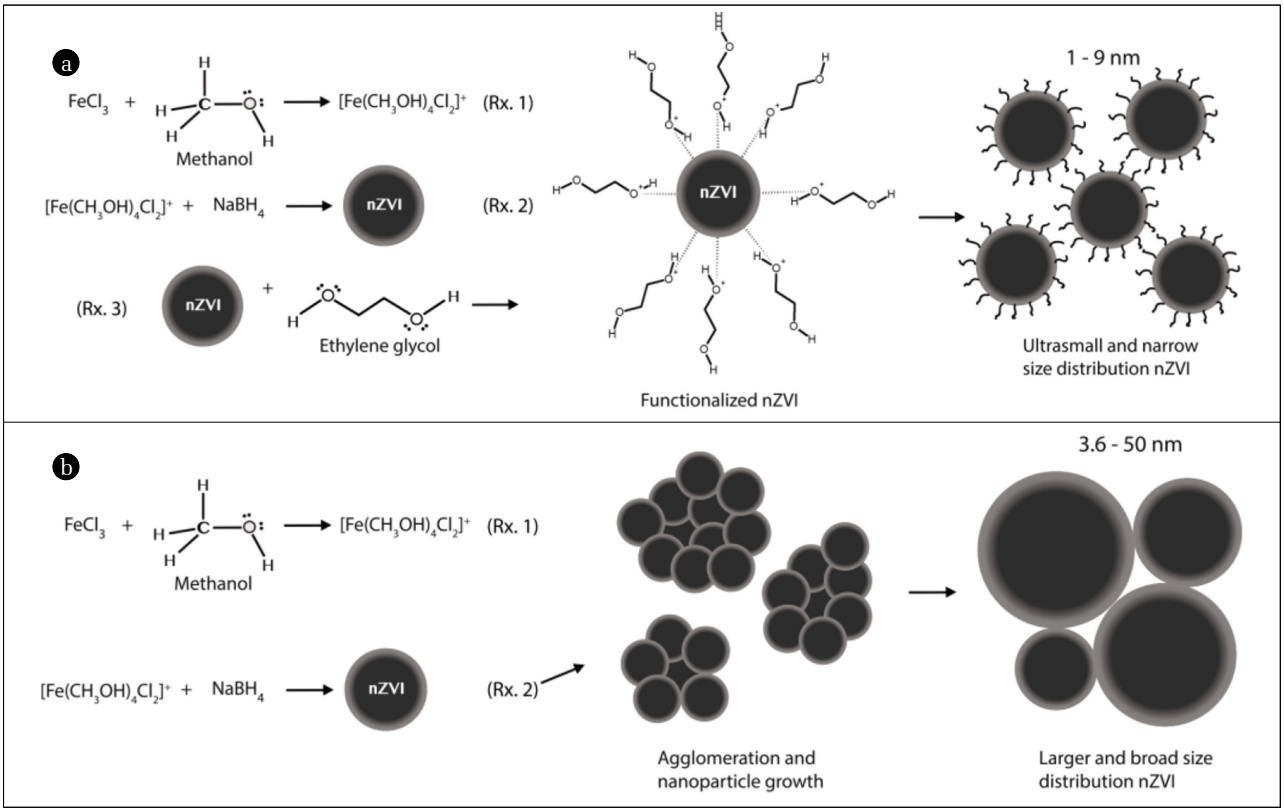

Fig. 2. Schematic illustration showing: (a) Fe^{3+} coordination process, functionalization of nZVI-EG_{non-aq} and size-control, (b) Fe^{3+} coordination and uncontrolled grow of S-$nZVI_{non-aq}$.

by occupying the empty d-orbitals of the metal by lone electron pairs of the ligand molecule, thereby generating the monodentate coordination of the surface of the nanoparticle and the graft of polymer chains.

With respect to the two mechanisms mentioned above, the use of non-aqueous solvent has an important role in particle stabilization with surface polymers. It is possible to achieve better grafting of the polymer brushes onto the particle surface, leading to better stabilization and control of the size using the chemical properties of methanol. When using a non-aqueous low polarity medium, it is possible to reduce the electrostatic hydrogen-bridge-type interactions between the solvent and the polymer employed during the synthesis for several reasons. First, there is a decrease in hydrogen bonding capacity in non-aqueous solvents (compared with aqueous solvents). This is associated with reduction of the H-bond length in methanol (0.956Å) compared with water (1.97Å) [28]. Second, there is decrease in the number of H sites available to interact in the non-aqueous solvent. This reduces electrostatic interaction and bond formation. Finally, higher polarity in aqueous type solvents results in higher probability of intermolecular bond formation between the molecules of the solvent and the polymer.

According to the information described above, and from the facts revealed by UV-Spectra and FTIR, we proposed obtaining ultra-small functionalized nanoparticles with narrow size distribution by the non-aqueous method. First, the methanol generated one stabilization mechanism via Fe^{3+} coordination due to reaction with methanol CH_3OH molecules to form a relatively stable complex $[Fe(CH_3OH)_4Cl_2]^+$ (Fig. 2(a): Rx. 1). The complex was then reduced with sodium borohydride ($NaBH_4$) to form nuclei and start the growth of the primary particles (Fig. 2(a): Rx. 2). However, a second mechanism of stabilization arose during the interaction of EG with the nanoparticles formed. This prevented particle agglomeration, made the synthesis of nZVI more efficient, and kept the size distribution narrower (Fig. 2(a): Rx. 3).

3.2. Size Control Using Non-aqueous Solvent with Stabilization Agent

3.2.1. Morphological characterization — Transmission electron microscopy (TEM)

The TEM images corresponding to the nZVI-EG_{non-aq} sample show a quasi-spherical morphology (Fig. 3(a)). In addition, it is possible to see an arrangement of nZVI in clusters mainly caused by the magnetic dipole-dipole interactions of the particles, generating an arrangement of these in a magnetic cluster. This type of arrangement has previously been reported for nZVI with similar sizes [5, 16]. Similarly, nanoparticles corresponding to the non-functionalized sample, present a quasi-spherical morphology (Fig. 3(b)). Notwithstanding, in contrast with the functionalized sample, a different arrangement in the alignment of particles is observed, where S-$nZVI_{non-aq}$ present particles arranged in chain-like structures

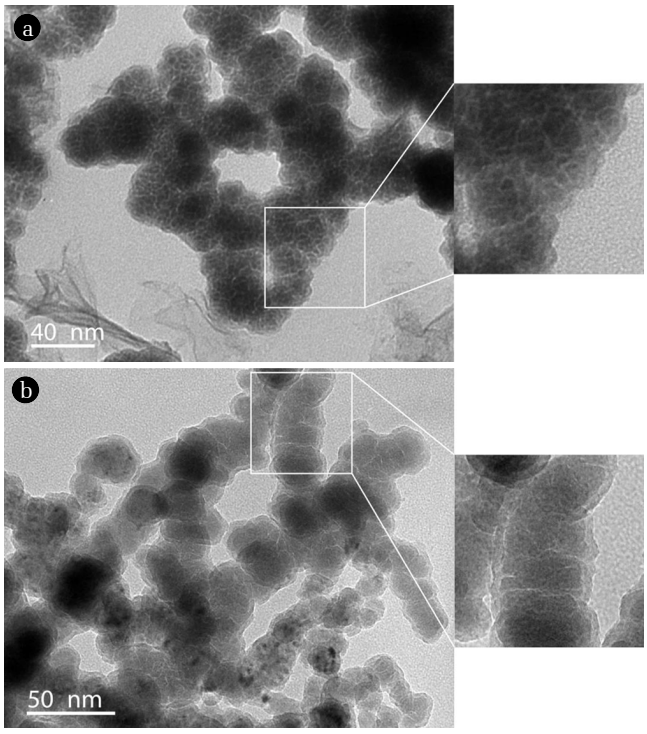

Fig. 3. a) TEM photomicrography of nZVI-EG_{non-aq}. b) TEM image of S-$nZVI_{non-aq}$.

due to the same magnetic attraction effects to which the particles are subjected. However, this arrangement of structures is a behavior typically shown by nanomaterials of this type [7, 9]. In addition, in our previous work, the formation of zero-valent iron nano-chains (in the presence and absence of a functionalizing agent, EG) was described in our previous study [15], which demonstrates that the nZVI arrangement in chain type structures is independent of particles surface modification, indicating that this behavior is directly related to the size and particle size distribution.

3.2.2. Size distribution analysis

Statistical analysis of the size distribution of the synthesized particles was carried out using the differential and cumulative distribution of the nZVI-EG_{non-aq}, $SnZVI_{non-aq}$, and nZVI-EG_{aq} diameters. Over 472 measurements were made using different TEM photomicrographs of the samples. The data corresponding to nZVI-EG_{aq} was acquired in our previous study [15]. The statistical parameters obtained are shown in Table S2.

The differential distribution was adjusted using a non-linear lognormal distribution model to model the entire range of population behavior, which is widely used as reference model in nanomaterial size distribution analysis due to the low coefficients of variation calculated in comparison with the different models used [29]. The differential particle size histogram corresponding to nZVI-EG_{non-aq} sample displays a particle diameter range of 1-9 nm, distributed in a normal manner with an asymmetrical geometry positively biased and a unimodal (single peak) distribution, but not monodisperse (all one size). The average particle size calculated for this model was 4.23 nm (Fig. 4(a)).

The range of the particle diameter for the synthesized S-$nZVI_{non-aq}$ sample initially showed a remarkable difference caused by the absence of the functionalizing agent (range 3.6-50 nm). The histogram showed a normal and asymmetrical geometry with a slight positive bias. The average diameter corresponding to this sample was 23.68 nm, a drastic increase in particle size compared with the first functionalized sample described, caused by the absence of stabilizing agent to avoid the uncontrolled particle growth. (Fig. 4(b)). The histogram corresponding to the sample synthesized in aqueous media in the presence of EG, nZVI-EG_{aq}, presented a normal geometry that was unimodal but partially symmetrical. This indicates a contrast with the previously described histograms. The particle sizes were in the range 16.9-100.2 nm, with average size of 55.14 nm. This marks a drastic increase compared to the samples obtained in non-aqueous solvent (Fig. 4(c)).

The central dispersion trend of the data distribution curve was evaluated using full width at half maximum (FWHM). For this work an absolute value of 2.81 nm was calculated in the range 2.66-5.47 nm, reflecting a low dispersion of the data population (Fig. 4(a)). For the non-functionalized sample (S-$nZVI_{non-aq}$), the central dispersion presents a much larger value (33.17 nm) within the range 9.91-43.08, demonstrating the widening of the size distribution from the absence of the EG (S-$nZVI_{non-aq}$; Fig. 4(b)). Finally, for the case of nZVI-EG_{aq}, the value corresponding to FWHM was 37.59 nm, within the range 39.44-77.03 nm. This value is close to that for S-$nZVI_{non-aq}$, indicating a similar size distribution for both cases (Fig. 4(c)). This is because, even though the diameter range of the particles was wider (16.9-100.2 nm), the size distribution was narrower due to the higher frequency of a smaller range of diameters are predominating. This could possibly be due to the effects of functionalization, and control of the size distribution by the presence of the polymer, EG, that modified the surface in these and produced steric repulsion effects [15]. In contrast, the sample S-$nZVI_{non-aq}$ showed a much wider size distribution, which can be seen in the histogram, indicating similar frequencies in the different particle sizes. This proves that the particle stabilization mechanism that occurred via coordination of Fe^{3+} ions by the organic molecules of the solvent generated a reduction in particle size (3.6-50 nm), however, control of the agglomeration and preservation of small diameters in these particles was not maintained, due to the absence of a stabilizing agent to saturate the particle surfaces.

Another technique by which to measure data propagation with respect to the arithmetic mean is use of the coefficient of variation (CV) or relative standard deviation (RSD). These are independent of the units and are expressed in percent, giving better visualization and understanding of the propagation of the independent variable with respect to the average value. The value obtained associated with nZVI-EG_{non-aq} for this analysis was < 7.5% (1-9 nm), indicating a quite narrow size distribution for materials of this type and a much greater value of < 60% (3.6-50 nm) corresponding to the broad size distribution of S-$nZVI_{non-aq}$ (Fig. 4(a) and (b)). The CV value obtained for nZVI-EG_{aq} was 27.8% (16.9-100.2 nm), which is nearly half of the value for S-$nZVI_{non-aq}$ (Fig. 4(c)), and better indicates the great difference in dispersion of the set of diameters analyzed. By obtaining this parameter, it is possible to appreciate the marked difference between the various size

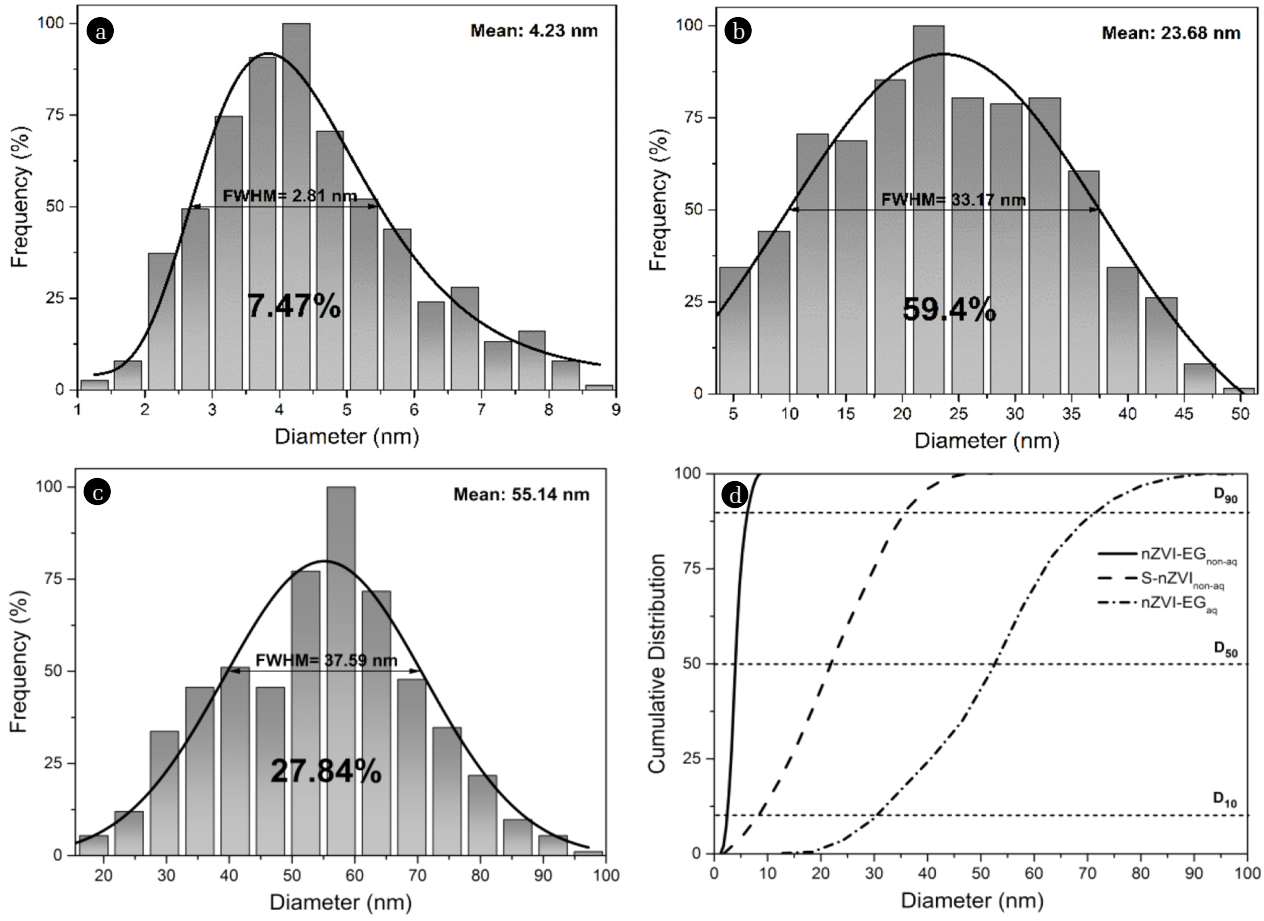

Fig. 4. Differential and cumulative size distribution of a) nZVI-$EG_{non\text{-}aq}$, b) S-$nZVI_{non\text{-}aq}$, c) nZVI-EG_{aq}, and d) Cumulative size distribution of the samples.

distributions. This corroborates the information explained above about the size dispersions for the samples S-nZVI and nZVI-EG_{aq}, and gives a better visualization of the predominance particle size regarding control of the narrow size distribution for nZVI-$EG_{non\text{-}aq}$.

The cumulative distribution of the particle sizes for the nZVI-$EG_{non\text{-}aq}$ sample shows that the distribution becomes narrower in sizes smaller than the median of the population (D_{50}), with a dispersion of 1.52 nm (D_{50}-D_{10}), indicating that 50% of the particles have diameters < 3.90 nm (Fig. 4(d)). On the other hand, it is observable that 90% of the measured data indicates particle sizes < 6.10 nm. The domain of particles with diameters smaller than this length implies good control of sizes during synthesis, and show little influence from particles with dimensions > D_{90} in the sample (6.10-9 nm; Fig. 4(d)). This corroborates better effectiveness from the use of both stabilization mechanisms.

In view of the information described above, the nZVI size-control presented is quite remarkable in relation to different methodologies reported previously that employed the use of aqueous or non-aqueous solvent, or a mixture of them. These differences are due to a variety of conditions such as poor size control, broad size distribution, complex synthesis methodologies, and the use of inert conditions [13, 17, 25].

3.2.3. Dynamic light scattering (DLS) and zeta potential

Table 1 shows the hydrodynamic radius obtained by DLS measurement (6.5 nm) for the nZVI-$EG_{non\text{-}aq}$ sample and 265.1 nm for S-$nZVI_{non\text{-}aq}$ without functionalization, where the large diameter of the latter corresponds to the magnetic clusters generated by the rapid aggregation of particles.

Moreover, the Z-potential for S-$nZVI_{non\text{-}aq}$ and nZVI-$EG_{non\text{-}aq}$ were measured with a value of +16.3 and −13.0 mV, respectively (Table 1). The difference in polarity of the Z-potential associated with nZVI-$EG_{non\text{-}aq}$ is due to the partial negative charge generates by the lone electron pairs contained in the terminal groups present in EG that are not linked to the particle surface. These attract positive countercharges, modifying the polarity of the hydrodynamic radius. However, despite the samples having opposite polarities, the values are in similar ranges. This shows that there is electrostatic repulsion between the nanoparticles, preventing their agglomeration and indicating that the force of attraction between the particles is only magnetic. This demonstrates that the stable nano-suspension of nZVI-$EG_{non\text{-}aq}$ and that small hydrodynamic conservation (6.5 nm) occur through the functionalization of the particles and the resulting effects from saturated surfaces and steric stabilization [12].

Table 1. Dynamic Light Scattering (DLS) and Zeta Potential of $nZVI_{non-aq}$ Samples

Sample	Particle size (nm)	Z potential (mV)
$nZVI\text{-}EG_{non-aq}$	6.5	+16.3
$S\text{-}nZVI_{non-aq}$	265.1	-13.0

3.2.4. Sedimentation analysis for nano-suspension stability examination

Sedimentation tests of the materials were carried out to show an increase in the colloidal stability, increase in dispersibility, reduction of the particle aggregation associated with the surface modification by the polymer brushes, and reduction in the diameter of the particles attributed to the different stabilization mechanisms used in this work. The curve was further analyzed using the one-phase decay equation, as described in our previous study [9].

$$I_t = I_0 e^{-t/\tau} \quad (1)$$

The curve associated with the $nZVI\text{-}EG_{non-aq}$ sample shows an insignificant sedimentation rate at two hours, indicating that > 90% of the particles remained in suspension during the sedimentation experiment. On the other hand, < 10% of the particles remained suspended with $S\text{-}nZVI_{non-aq}$, indicating very rapid sedimentation (Fig. 5). The characteristic time τ for the samples in the presence and absence of a functionalizing agent were calculated to be 1993 and 43.84 min, respectively, a difference of about 45 times. Associated with this information, Hwang et al. [9] described that the increase in characteristic time is directly related to reduction in the hydrodynamic radius and by the decreasing stress due to the size of the suspended particle. This explains why $nZVI\text{-}EG_{non-aq}$ particles had such high colloidal stability.

In fact, the continued suspension of > 90% of the particles could be related to the size distribution analysis, by which it was seen that > 90% of particles had sizes < 6.10 nm. Quite possibly, the greater colloidal stability was due to their size. However, these particles can be attracted magnetically, and are still subject to eventual sedimentation. The saturation of the surface of the nanoparticles and the existence of steric repulsion from their functionalization, increased the dispersibility, delayed agglomeration, and hindered sedimentation of the particles [15, 30].

Furthermore, it has been reported that higher Fe(0) content in the particles was associated with greater force of magnetic attraction, which could generate more rapid aggregation of the particles [21]. In view of this, the remarkable increase in the sedimentation rate for simple $nZVI_{non-aq}$ (in relation to the sample described above) is related to the increment in diameter of the particles. This is because a magnetic moment of greater magnitude is associated with larger nZVI [4], and would be expected to increase the magnetic attraction between particles. To illustrate this, consider that if the diameter of particles in a sample were larger, the magnetic cores and core-shells made of magnetite would have larger dimensions and thereby, greater magnetic force. Therefore, greater interaction and attraction would exist between the particles. From this, follows the formation of large fractal aggregates in chain-like structures, as explained in the DLS description. These would settle more rapidly; so that, even though

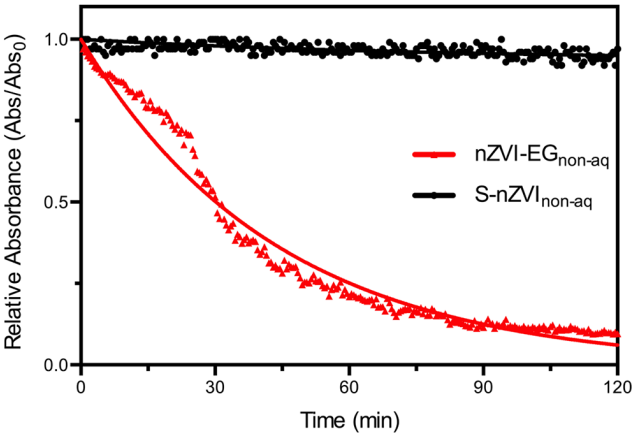

Fig. 5. Sedimentation curves of nZVI and nZVI-EG.

10% of the particles had diameters < 8.31 nm (which might confer greater colloidal stability due to their size); they could also easily be attracted by larger diameter particles present because of the wide size distribution, and subsequently be subjected to sedimentation.

The anti-aggregation capacity and the very high colloidal stability of $nZVI\text{-}EG_{non-aq}$ were compared with previous reports. In the other cases, even with low Fe(0) content in the particles, low concentration of nZVI in the sedimentation tests, and similar particle sizes, the nZVI quickly agglomerated in solution, leading to precipitates and therefore did not show stability even close to the values presented in this work [5, 21]. Therefore, these results highlight the properties of our new material and its applicability for environmental remediation, particularly for in situ subsurface remediation, due to the potentially high mobility of the nanomaterial in groundwater.

3.3. Effect of Functionalization in Reactivity of nZVI

3.3.1. X-ray diffraction

The X-ray diffractogram corresponding to $nZVI\text{-}EG_{non-aq}$ shows the characteristic peak of the body-centered cubic (bcc) phase α-Fe located at 44.8°, which can be indexed as the (110) plane (JCPDS Card No. 79-0417). Diffraction patterns revealed a peak corresponding to the crystallographic phase magnetite (Fe_3O_4) at 35.4° indexed in the plane (311) (JCPDS 06-0696) that compounds the iron oxide core-shell that surrounds α-Fe. In a similar way, the spectrum of $S\text{-}nZVI_{non-aq}$ presents with lower intensity the peak corresponding to α-Fe and a magnetite peak with greater intensity. Moreover, the diffracted peaks associated with sample $nZVI\text{-}EG_{aq}$, represent the same crystallographic phases. However, there was marked increase in intensity and width related to better crystallinity of the material (Fig. 6).

In the Rietveld refinement of the XRD information is presented a greater percentage of the metal nucleus α-Fe and a smaller proportion of magnetite for the functionalized samples, compared with the simple non-aqueous sample (Table S3). This conservation of the nucleus is due to the presence of the functionalizing agent, which prevented the additional oxidation of α-Fe [15]. Nevertheless, for non-aqueous samples, even if the methanol could

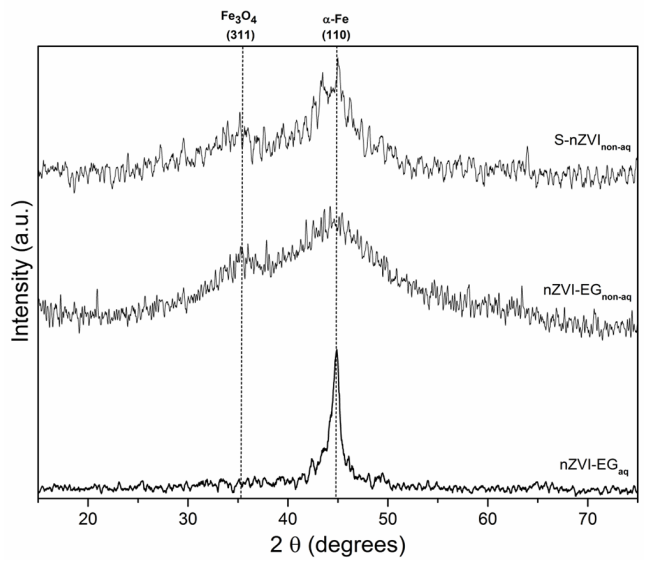

Fig. 6. XRD patterns of S-nZVI and nZVI-EG.

reduce this effect, the interaction of the material with the surrounding environment would occur owing to the increased reactivity caused by the particle size reduction. In light of this, the higher iron core conservation of nZVI-EG_{aq} is explained by the larger particle sizes. In the XRD pattern, the peaks corresponding to non-aqueous samples have a remarkable width. This widening of the peaks, a behavior seen in materials of this type, was previously noted when the synthesis of nZVI in water, ethanol, and in mixtures of different proportions were reported. This demonstrated the stabilization and reduction of the particle size in the nanomaterials according to increase in the ethanol used as solvent. This was reflected in a widening of the diffracted peaks for particles with smaller dimensions. This was associated with decrease in the particle size and spreading of the peaks in XRD. This is because reduction in the size of the crystals increased the number of defects in the crystalline network in response to the smaller number of atoms available to assemble the crystallite. Due to the defects and the size, diffraction peaks of the crystallites show less intensity and a widening respect to peaks corresponding to crystals much bigger and free-defect [31]. Despite the widening of both spectra, a greater widening of the peaks was shown for nZVI-EG. This can be related to decrease of the diameter of the particles and the crystals, explaining the much greater crystallinity of nZVI-EG_{aq}, as shown in its higher intensity and wider peaks. Even with the widening of the diffracted peaks, it was possible to see better crystallinity for non-aqueous nanomaterials compared with amorphous nZVI of similar diameters reported before. This is because it is possible to detect the peaks associated with the different crystallographic phases present in the samples [16, 25]. However, the low intensity of the XRD pattern of sample makes difficult the calculation of the crystalline size to corroborate this.

3.3.2. Reactive iron content

The amount of reactive iron in the synthesized samples indicates the degree of oxidation of the metal core, thereby demonstrating the stability of the particles during synthesis, using methanol

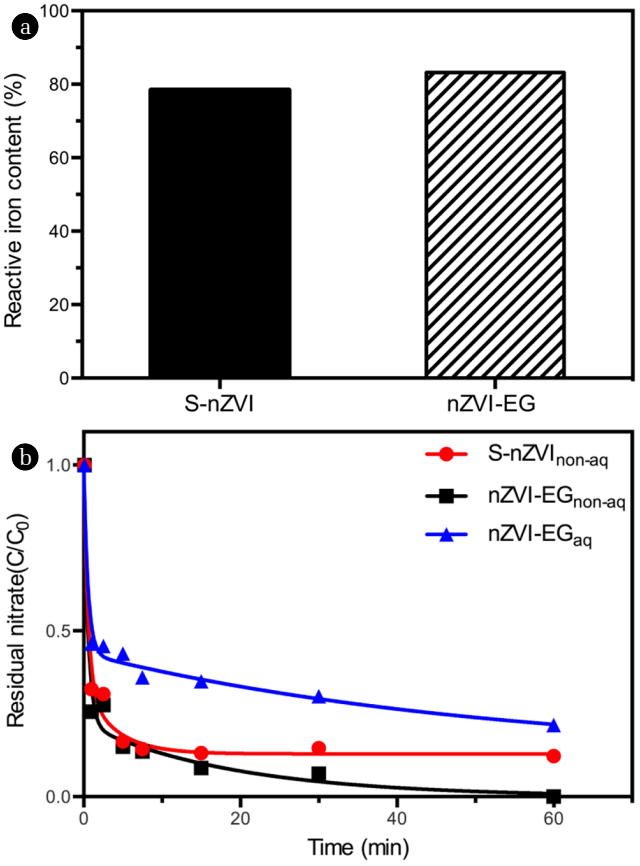

Fig. 7. a) Reactive iron content of nZVI samples, b) Nitrate reduction by nZVI samples (Conditions: 12.5 mg NO_3-N/L and 1,000 mg Fe/L, pH 5, T = 24 ± 1°C).

as solvent, without the need for inert conditions. The percentage of elemental iron for samples (S-nZVI$_{non-aq}$) without functionalization presented a value of 78.4% (83.2% for nZVI-EG$_{non-aq}$). Both percentages confirmed high conservation of the reactive nucleus in the absence of inert atmosphere (Fig. 7(a)). For this reason, taking as reference the reactive iron content obtained in the aqueous phase described in the previous study, the percentages of Fe(0) obtained in this work are similar. However, even though the use of methanol preserved the metal core, the loss of > 15% of Fe(0) in the materials was related to the high reactivity rate of the particles with the surrounding medium. This is because there was a notable difference in the materials compared, in relation to size and particle size distribution, which is directly related to increase of the surface area and the reactivity of these.

3.3.3. Nitrate reduction

In this study, nitrate was selected as a model compound to confirm the reducing reactivity of nZVI. It is well-known that nitrate is reduced to ammonia by reaction with ZVI; therefore, we measured the ammonia concentration to monitor the nitrate reduction. Fig. 7(b) presents the nitrate reduction profile of the three different nZVIs tested, and shows the effect of methanol and/or the stabilizing agent (EG). The nZVI synthesized in non-aqueous solvent

showed much higher reactivity at the beginning of reaction. For example, > 70% of the nitrate was removed in the first minute of reaction, indicating almost instant reaction between nZVI and nitrate. On the other hand, the nZVI synthesized in aqueous solvent only reduced ~ 50% of the nitrate in the same time. Therefore, we saw clear benefits for non-aqueous solvent (methanol) on nZVI reactivity due to decrement of particle size.

Moreover, nZVI-$EG_{non\text{-}aq}$ showed better reactivity than did S-$nZVI_{non\text{-}aq}$, even though they were both synthesized in methanol. Continuous nitrate reduction was achieved with nZVI-$EG_{non\text{-}aq}$, by which all the nitrate was reduced in one hour. On the other hand, no more reduction occurred in S-$nZVI_{non\text{-}aq}$ after 15 min of reaction. This result corresponded well with the sedimentation curve. The S-nZVI particles aggregated, especially at 20-30 min, indicating formation of large clusters, not individual particles. The large clusters inhibit mass transfer as well as overall reaction; therefore, the reaction was slowed after aggregation. Using functionalized nZVI in non-aqueous solvent promises rapid initial reaction due to the small particle size and narrow size distribution, as well as its long-term reactivity due to low aggregation during reaction.

4. Conclusions

In this study, methanol (non-aqueous solvent) and ethylene glycol were investigated as stabilizing mechanisms for the synthesis of ultra-small, size-controlled nZVI without inert conditions. The first mechanism of stabilization occurs by coordination of iron ions by MEOH molecules, which were further reduced to Fe(0). Subsequently, the second stabilization mechanism occurs by surface modification by grafting of EG brushes onto the particles. This combination generated a narrow particle size distribution nZVI (< 7.5%): 90% of the particles had sizes < 6.1 nm. After the functionalization process, they exhibited extremely high dispersibility in water, which was confirmed by stability testing by sedimentation analysis and DLS. Even in the absence of inert conditions during synthesis, the XRD and iron reactive content analyzes showed high conservation of the Fe(0) reactive nucleus. Reactivity tests on the reduction of nitrates showed that higher reactivity was observed toward the contaminant in solution, which was associated with great colloidal stability from both the ultra-small diameters and narrow particle size distribution.

Acknowledgments

This work is supported by Korea Ministry of Environment as “The SEM projects; 2018002480004”. Claudio Adrian Ruiz-Torres would like to thank to Consejo Nacional de Ciencia y Tecnología (CONACYT) for its support with the scholarship No. 412287.

References

1. Fu F, Dionysiou DD, Liu H. The use of zero-valent iron for groundwater remediation and wastewater treatment: A review. *J. Hazard. Mater.* 2014;267:194-205.
2. Stefaniuk M, Oleszczuk P, Ok YS. Review on nano zerovalent iron (nZVI): From synthesis to environmental applications. *Chem. Eng. J.* 2016;287:618-632.
3. Suslick KS, Fang M, Hyeon T. Sonochemical synthesis of iron colloids. *J. Am. Chem. Soc.* 1996;118:11960-11961.
4. Farrell D, Majetich SA, Wilcoxon JP. Preparation and characterization of monodisperse Fe nanoparticles. *J. Phys. Chem. B.* 2003;107:11022-11030.
5. Huber DL, Venturini EL, Martin JE, Provencio PP, Patel RJ. Synthesis of highly magnetic iron nanoparticles suitable for field structuring using a β-diketone surfactant. *J. Magn. Magn. Mater.* 2004;278:311-316.
6. Khalil H, Mahajan D, Rafailovich M, Gelfer M, Pandya K. Synthesis of zerovalent nanophase metal particles stabilized with poly(ethylene glycol). *Langmuir* 2004;20:6896-6903.
7. Sun Y, Li X, Cao J, Zhang W, Wang HP. Characterization of zero-valent iron nanoparticles. *Adv. Colloid Interface Sci.* 2006;120:47-56.
8. Azzam AM, El-Wakeel S, Mostafa BB, El-Shahat M. Removal of Pb, Cd, Cu and Ni from aqueous solution using nano scale zero valent iron particles. *J. Environ. Chem. Eng.* 2016;4: 2196-2206.
9. Hwang Y, Lee Y, Mines PD, Huh YS, Andersen HR. Nanoscale zero-valent iron (nZVI) synthesis in a Mg-aminoclay solution exhibits increased stability and reactivity for reductive decontamination. *Appl. Catal. B-Environ.* 2014;147:748-755.
10. Kanel SR, Manning B, Charlet L, Choi H. Removal of arsenic(III) from groundwater by nanoscale zero-valent iron. *Environ. Sci. Technol.* 2005;39:1291-1298.
11. Liu A, Liu J, Han J, Zhang W. Evolution of nanoscale zero-valent iron (nZVI) in water: Microscopic and spectroscopic evidence on the formation of nano- and micro-structured iron oxides. *J. Hazard. Mater.* 2017;322:129-135.
12. Lee N, Choi K, Uthuppu B, et al. Synthesis of iron nanoparticles with poly(1-vinylpyrrolidone-co-vinyl acetate) and its application to nitrate reduction. *Adv. Environ. Res.* 2014;3:107-116.
13. Sun Y, Li X, Zhang W, Wang HP. A method for the preparation of stable dispersion of zero-valent iron nanoparticles. *Colloids Surf. A. Physicochem. Eng. Asp.* 2007;308:60-66.
14. He F, Zhao D. Preparation and characterization of a new class of starch-stabilized bimetallic nanoparticles for degradation of chlorinated hydrocarbons in water. *Environ. Sci. Technol.* 2005;39:3314-3320.
15. Ruiz-Torres CA, Araujo-Martínez RF, Martínez-Castañón GA, et al. Preparation of air stable nanoscale zero valent iron functionalized by ethylene glycol without inert condition. *Chem. Eng. J.* 2018;336:112-122.
16. Wang Q, Snyder S, Kim J, Choi H. Aqueous ethanol modified nanoscale zerovalent iron in bromate reduction: Synthesis, characterization, and reactivity. *Environ. Sci. Technol.* 2009;43:3292-3299.
17. Lowry GV, Johnson KM. Congener-specific dechlorination of dissolved PCBs by microscale and nanoscale zerovalent iron in a water/methanol solution. *Environ. Sci. Technol.* 2004;38: 5208-5216.
18. Ambika S, Nambi IM. Optimized synthesis of methanol-assisted nZVI for assessing reactivity by systematic chemical

speciation approach at neutral and alkaline conditions. *J. Water Process Eng.* 2016;13:107-116.
19. Pan D, Ji X, An L, Lu Y. Observation of nucleation and growth of CdS nanocrystals in a two-phase system. *Chem. Mater.* 2008;20:3560-3566.
20. Brillo J, Pommrich AI, Meyer A. Relation between self-diffusion and viscosity in dense liquids: New experimental results from electrostatic levitation. *Phys. Rev. Lett.* 2011;107:165902.
21. Phenrat T, Saleh N, Sirk K, Tilton RD, Lowry GV. Aggregation and sedimentation of aqueous nanoscale zerovalent iron dispersions. *Environ. Sci. Technol.* 2007;41:284-290.
22. Liu Y, Majetich SA, Tilton RD, Sholl DS, Lowry GV. TCE dechlorination rates, pathways, and efficiency of nanoscale iron particles with different properties. *Environ. Sci. Technol.* 2005;39:1338-1345.
23. Hwang Y, Salatas A, Mines PD, Jakobsen MH, Andersen HR. Graduated characterization method using a multi-well microplate for reducing reactivity of nanoscale zero valent iron materials. *Appl. Catal. B-Environ.* 2016;181:314-320.
24. Drago RS, Hart DM, Carlson RL. Spectrophotometric studies of iron(III) chloride in nonaqueous solvents. *J. Am. Chem. Soc.* 1965;87:1900-1904.
25. Dinç M, Metin Ö, Özkar S. Water soluble polymer stabilized iron(0) nanoclusters: A cost-effective and magnetically recoverable catalyst in hydrogen generation from the hydrolysis of sodium borohydride and ammonia borane. *Catal. Today* 2012;183:10-16.
26. Kurata M, Yamakawa H, Teramoto E. Theory of dilute polymer solution. I. Excluded volume effect. *J. Chem. Phys.* 1958;28:785-792.
27. Wertz DL, Kruh RF. Structure of iron(III) chloride-methanol solutions. *J. Chem. Phys.* 1969;50:4013-4018.
28. Zhang N, Shen Z, Chen C, He G, Hao C. Effect of hydrogen bonding on self-diffusion in methanol/water liquid mixtures: A molecular dynamics simulation study. *J. Mol. Liq.* 2015;203:90-97.
29. Rice S, Chan C, Brown S, et al. Particle size distributions by transmission electron microscopy: An interlaboratory comparison case study. *Metrologia* 2013;50:663.
30. Sperling RA, Parak WJ. Surface modification, functionalization and bioconjugation of colloidal inorganic nanoparticles. *Philos. Trans. Roy. Soc. A.* 2010;368:1333-1383.
31. Chen S, Zhang Y, Han W, Wellburn D, Liang J, Liu C. Synthesis and magnetic properties of Fe_2O_3-TiO_2 nano-composite particles using pulsed laser gas phase evaporation-liquid phase collecting method. *Appl. Surf. Sci.* 2013;283:422-429.